8

CHAPTER 8: CONSTRUCTAL FLOW ORIENTATION IN CONJUGATE COOLING CHANNELS WITH INTERNAL HEAT GENERATION[6]

8.1. INTRODUCTION

This chapter presents the development of a three-dimensional flow architecture of conjugate cooling channels in forced convection - with internal heat generation within the solid - for an array of circular cooling channels with different flow orientation. Three flow orientations were studied: firstly an array of channels with parallel flow; secondly, array of channels in which the flow in every second row is in an opposite direction to its neighbours, and thirdly, an array of channels in which every row is in counter flow relative to each other. The geometric configurations were determined in such a way that the peak temperature was minimised, subject to the constraint of fixed the global volume of solid material. The degrees of freedom of the design were the hydraulic diameter of the channel and channel-to-channel spacing. A gradient-based optimisation algorithm was applied to search for the best optimal geometric

[6] This research section is published in part: T. Bello-Ochende, O.T. Olakoyejo, and J.P Meyer; "Constructal flow orientation in conjugate cooling channels with internal heat generation", *International Journal of Heat and Mass Transfer*, Vol. 57, pp. 241 - 249, 2013

configurations that would improve thermal performance by minimising thermal resistance for a wide range of dimensionless pressure differences. The effect of porosities, applied pressure difference, flow orientation and heat generation rate on the optimal hydraulic diameter and channel-to-channel spacing is reported. The results show that the effects of dimensionless pressure drop on minimum thermal resistance were consistent with those obtained in the open literature.

8.2. COMPUTATIONAL MODEL

Figure 8.1 shows the three flow orientations studied. The system consists of a solid body of fixed global volume *V*, which experiences uniform volumetric heat generation q_s'''. The body is cooled by forcing a single-phase cooling fluid (water) from the left side through the parallel cooling channels. The flow is driven along the length *L* of the circular channel with a fixed pressure difference ΔP. An elemental volume shown in Figure 8.2 consisting of four (4) cooling channels and the surrounding solid was accounted for by making use of symmetry and periodic boundary conditions. The heat transfer in the elemental volume is a conjugate problem, which combines heat conduction in the solid and the convection in the flowing fluid.

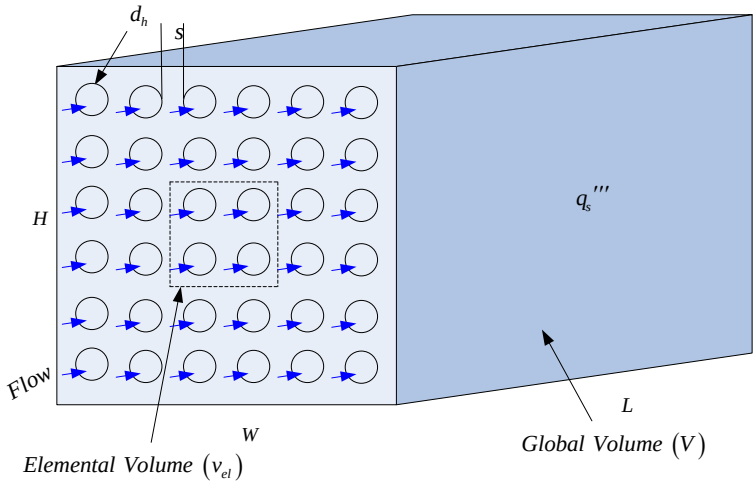
d_h
s
H
q_s'''
Flow
L
W
Global Volume (V)
Elemental Volume (v_{el})

(a)

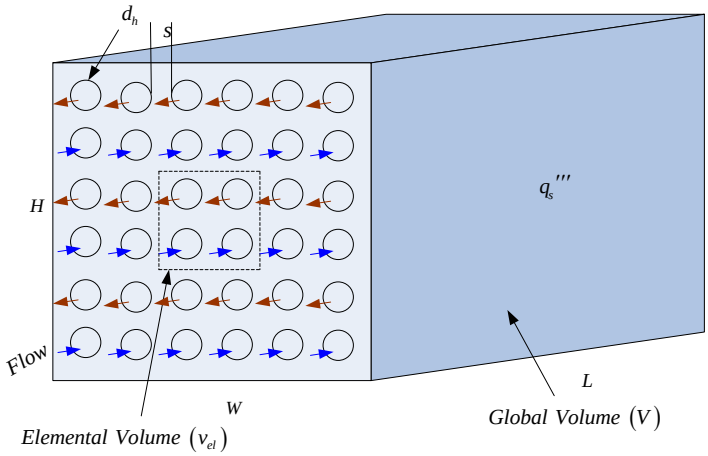
d_h
s
H
q_s'''
Flow
L
W
Global Volume (V)
Elemental Volume (v_{el})

(b)

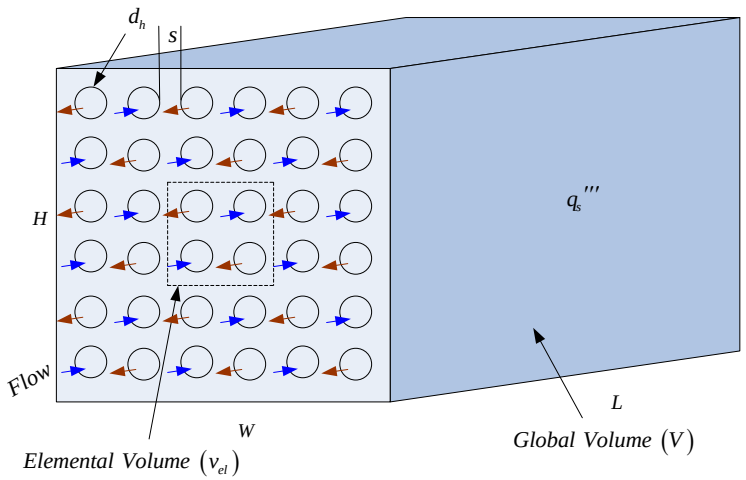

(c)

Figure 8. 1 : Three-dimensional parallel circular of (a) PF-1, (b) CF-2 and (c) CF-3 orientations

8.2.1. Design variables

In Figure 8.2, an elemental volume constraint v_{el} is composed of four circular cooling channels of equal hydraulic diameter d_h. The surrounding solid of thickness s (equal spacing between all channels) means that

$$w = h \tag{8.1}$$

The elemental volume is:

$$v_{el} = w^2 L \tag{8.2}$$

and the volume of a channel is

$$v_c = \frac{\pi}{4} d_h^{\,2} L \tag{8.3}$$

For a fixed length of the channel, the cross-sectional area of the structure is

$$A_s = HW \tag{8.4}$$

which means that the number of channels in the structure arrangement is

$$N = \frac{HW}{hw} \tag{8.5}$$

The void fraction (or porosity) of the elemental structure is defined as

$$\phi = 4\frac{v_c}{v_{el}} \tag{8.6}$$

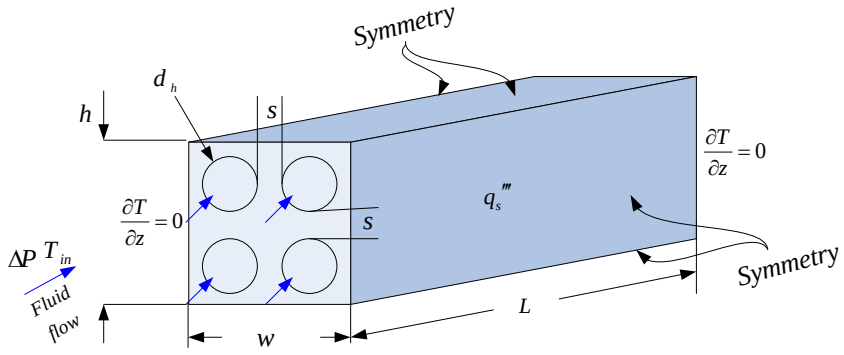

(a)

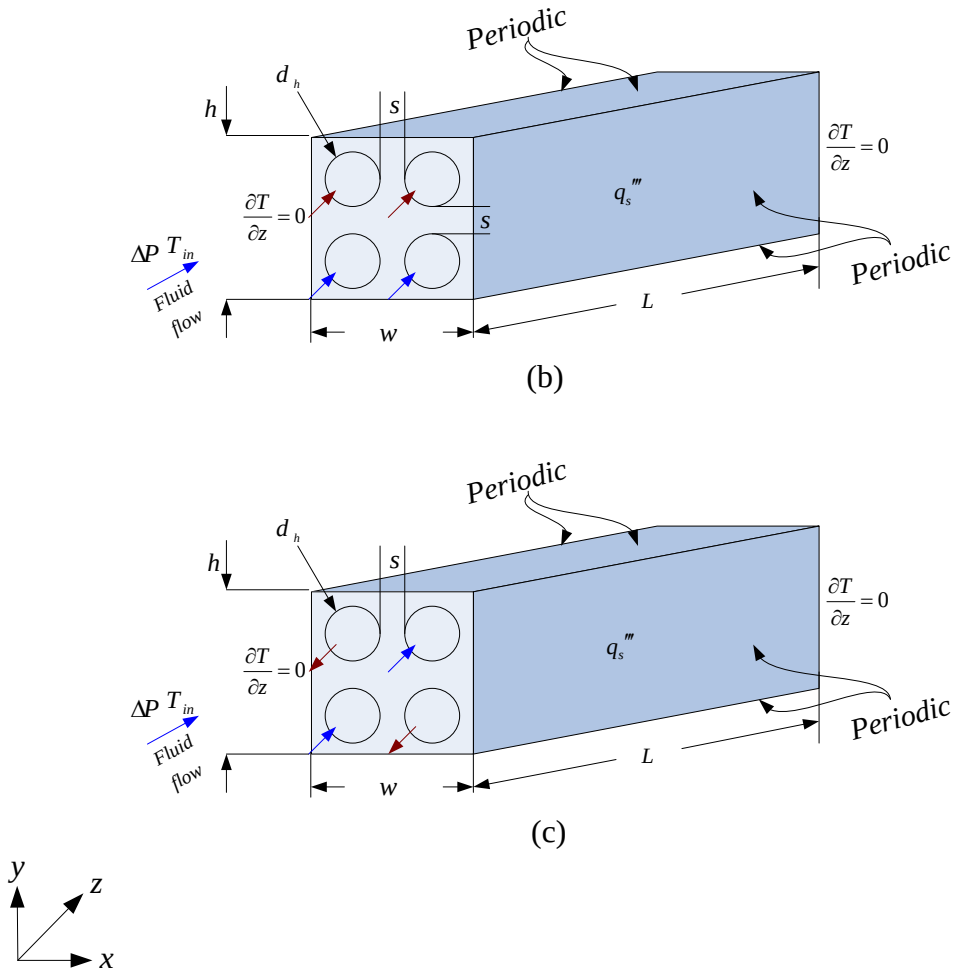

Figure 8. 2 : The boundary conditions of the three-dimensional computational domain of the elemental volume of (a) PF-1, (b) CF-2 and (c) CF-3 orientations

The objective is to find the channel hydraulic diameter d_h and the channel spacing s which offer minimum resistance to heat and flow. The analysis also focuses on the extreme limits of $0 \le d_h \le \infty$ and the extreme limits of $0 \le s \le \infty$.

The cooling fluid was water, which was forced through the cooling channels by a specified pressure difference ΔP across the flow length of the structure. The working

fluid was assumed to be in single phase, steady and Newtonian with constant properties.

Other assumptions imposed on the configuration models were the following: For the PF-1 configuration, the top, bottom, left and right boundaries of the domain corresponded to symmetry boundary conditions. For CF-2 and CF-3, the top, bottom, left and right side of the solid surfaces had spatially periodic thermal boundary conditions. The remaining outside walls and the plane of symmetry were modelled as adiabatic.

The measure of performance was the global thermal resistance, which is expressed in a dimensionless form in Equation (6.13) and it is a function of the optimised design variables, the peak temperature and flow orientations. Thus:

$$R_{\min} = f\left(d_{h_{opt}},\ s_{opt},\ v_{el_{opt}},\ T_{\max_{\min}},\quad \textit{flow orientation}\right) \tag{8.7}$$

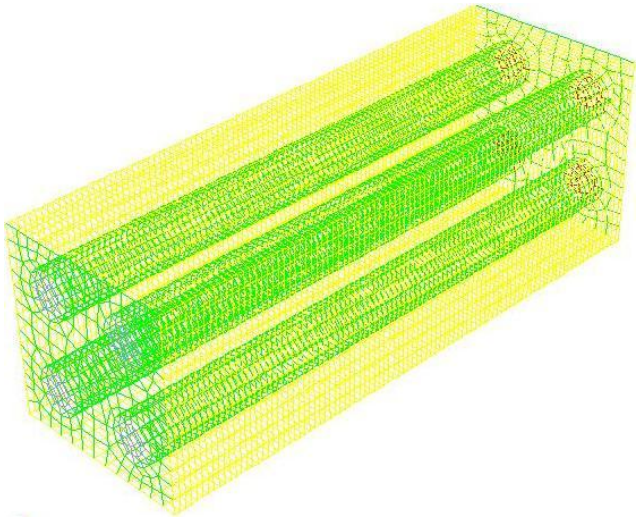

(a)

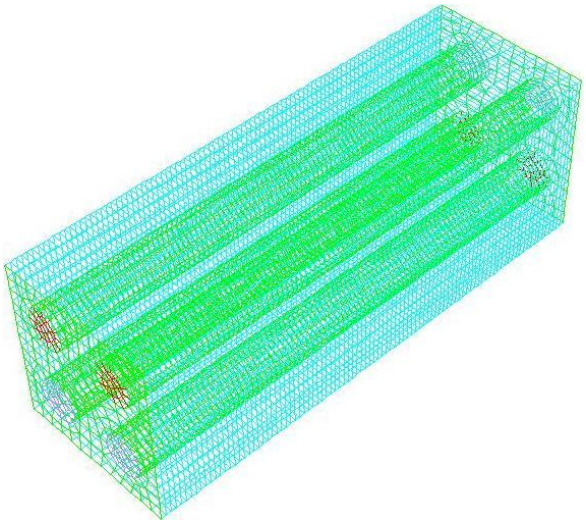

(b)

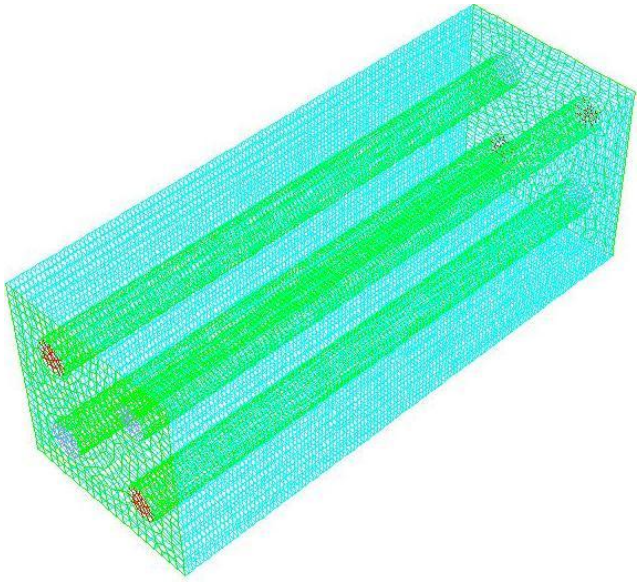

(c)

Figure 8. 3 : The discretised 3-D computational domains of (a) PF-1, (b) CF-2 and (c) CF-3 orientations

8.3. NUMERICAL PROCEDURE

The simulation work began by fixing the channel length, pressure difference, porosity, and heat generation rate, and varying the geometry and flow orientation to identify the configuration that decreased the peak temperature. The numerical solutions of temperature distribution in the elemental volume of each flow orientation configuration were obtained by solving the continuity, momentum and energy equations (Equations (3.1) to (3.8) of Chapter 3) along with the boundary conditions (Equations (8.1) to (8.6)) by using a three-dimensional commercial package Fluent™

[199], which employs a finite volume method. The details of the method are explained by Patankar [203]. Fluent™ was coupled with the geometry and mesh generation package Gambit [201] using MATLAB [219] to allow the automation and running of the simulation process. The computational domain was discretised using hexahedral/wedge elements. A second-order upwind scheme was used to discretise the combined convection and diffusion terms in the momentum and energy equations. The SIMPLE algorithm was then employed to solve the coupled pressure-velocity fields of the transport equations. The solution is assumed to have converged when the normalised residuals of the mass and momentum equations fall below 10^{-6} while the residual convergence of the energy equation was set to less than 10^{-10}. After the simulation had converged, an output file was obtained containing all the necessary simulation data and results for the post-processing and analysis.

The GAMBIT [201] journal files for the three flow orientation configurations are provided in Appendices B.7 to B.9 respectively. FLUENT [199] journal file in Appendix C is applicable to the simulations and need little modification.

8.4. GRID ANALYSIS AND CODE VALIDATION

To ensure accurate results, several grid independence tests were conducted until a mesh size with negligible changes in peak temperature was obtained. The number of grid cells used for the simulations varied for different elemental volume and

porosities. However, grid independence tests for several mesh refinements were carried out to ensure the accuracy of the numerical results. The convergence criterion for the overall thermal resistance as the quantity monitored is given as in Equation (6.15).

Tables 8.1 to 8.3 show the grid independence test for the PF-1, CF-2 and CF-3 configurations respectively with $v_{el} = 2.5\ \text{mm}^3$, $\phi = 0.2$ and $\Delta P = 50\ kPa$. The number of cells were 20 400, 36 186, 61 410 and 162 400 for the PF-1 orientation configuration. It is observed that almost identical results were predicted when 61 410 and 162 400 cells were used. Therefore, a further increase in the cell density beyond 61 410 has a negligible effect on the numerical result. The number of cells were 39 960, 43 000, 61 410 and 162 400 for both the CF-2 and CF-3 configurations.

Table 8. 1 : Grid independence study for the PF-1 configuration with $v_{el} = 2.5\ \text{mm}^3$, $\phi = 0.2$ and $\Delta P = 50\ kPa$

Number of nodes	Number of cells	$T_{\max}$	$\gamma = \dfrac{\left\|(T_{\max})_i - (T_{\max})_{i-1}\right\|}{\left\|(T_{\max})_i\right\|}$
31 091	20 400	27.77	-
50 318	36 186	27.754	0.000577
81 644	61 410	27.764	0.000216
204 783	162 400	27.764	0.000144

Table 8. 2 : Grid independence study for the CF-2 configuration with v_{el} = 2.5 mm^3 , ϕ = 0.2 **and** $\Delta P = 50\ kPa$

Number of nodes	Number of cells	$T_{\max}$	$\gamma = \frac{\left\|(T_{\max})_i - (T_{\max})_{i-1}\right\|}{\left\|(T_{\max})_i\right\|}$
54 109	39 960	27.671	-
59 909	43 000	27.670	0.00000325
81 644	61 410	27.693	0.000827
204 783	162 400	27.709	0.000577

Table 8. 3 : Grid independence study for the CF-3 configuration with v_{el} = 2.5 mm^3 ϕ = 0.2 **and** $\Delta P = 50\ kPa$

Number of nodes	Number of cells	$T_{\max}$	$\gamma = \frac{\left\|(T_{\max})_i - (T_{\max})_{i-1}\right\|}{\left\|(T_{\max})_i\right\|}$
54 109	39 960	27.671	-
59 909	43 000	27.672	0.00000361
81 644	61 410	27.694	0.000794
204 783	162 400	27.710	0.000577

It was worthy to note that almost identical convergence performance emerged when 61 410 and 162 400 cells were used. Therefore, a further increase in the cell density beyond 61 410 had a negligible effect on the numerical result.

8.5. NUMERICAL RESULTS

The elemental volume of the structure varied in the range of 0.125 mm^3 to 20 mm^3, and the porosity range was between $0.1 \leq \phi \leq 0.3$. The length was fixed at L = 10 mm, and the applied pressure difference was specified as $\Delta P = 50\ kPa$. The thermal conductivity of the solid structure (silicon) was 148 W/m.K, and the internal heat generation within the solid was taken to be fixed as 100 W/cm^3. The thermo-physical properties of water [202] used in this study was for water at 300 K and the inlet water temperature was fixed at this temperature.

Figures 8.4 and 8.5 show the existence of an optimum hydraulic diameter and elemental volume size in which the peak temperature is minimised at any point in the channel for the square configuration studied. Figure 8.4 shows the peak temperature as a function of the dimensionless channel hydraulic diameter. It also confirms existence of an optimal channel hydraulic diameter that lies in the range $0.005 \leq d_h/L \leq 0.025$ and minimises the peak temperature.

The elemental volume of the structure has a strong effect on the peak temperature as shown in Figure 8.5. The minimum peak temperature is achieved when the elemental volume is in the range $0.5\ mm^3 \leq v_{el} \leq 8\ mm^3$. This indicates that the global peak temperature decreases as the design variables (hydraulic diameter and elemental volume) increase or the global peak temperature decreases as the design variables decrease until it gets to the optimal design values. Therefore, any increase or decrease

in the design variable beyond the optimal values indicates that the working fluid is not properly engaged in the cooling process, which is detrimental to the global performance of the system.

The results show that the optimal arrangement of the elemental volume for the entire structure at this fixed pressure difference should be very small in order to achieve a better cooling. The results also show that the flow orientation has a strong influence on the convective heat transfer as the peak temperature is lower in the two counter-flow arrangements compared to their parallel-flow counterpart. What's more, the two counter-flow arrangements show almost the same performance. However, the peak temperature of the CF-2 orientation is slightly lower (if $d_h/L < 0.01$) than that of the CF-3 orientation.

According to Figures 8.4 and 8.5, porosity has a significant effect on the peak temperature. The best cooling occurs at the highest porosity. Thus, as the porosity increases, the peak temperature decreases. Furthermore, when the porosity increases the flow direction has almost no impact on the results. This means that this research finds its application in low porosity designs.

.

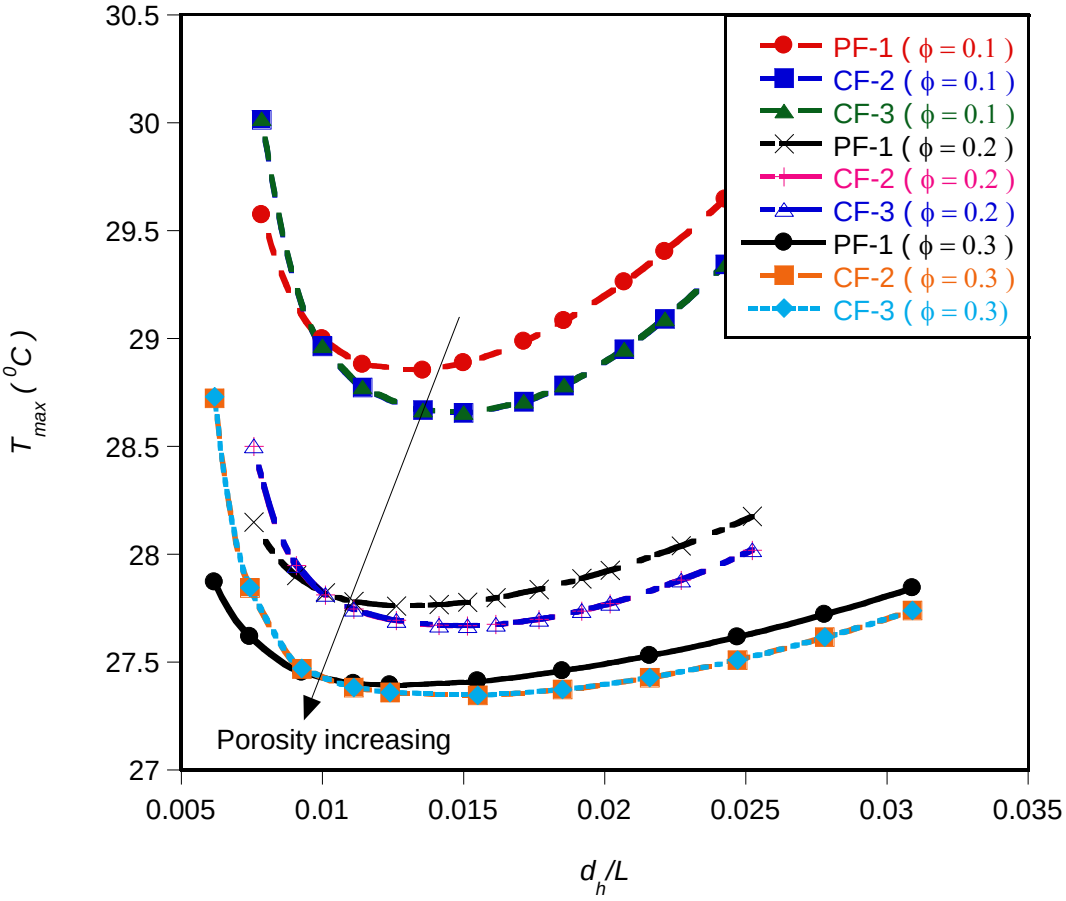

Figure 8. 4 : Effect of the optimised dimensionless hydraulic diameter d_h on the peak temperature at ΔP = 50 *kPa*

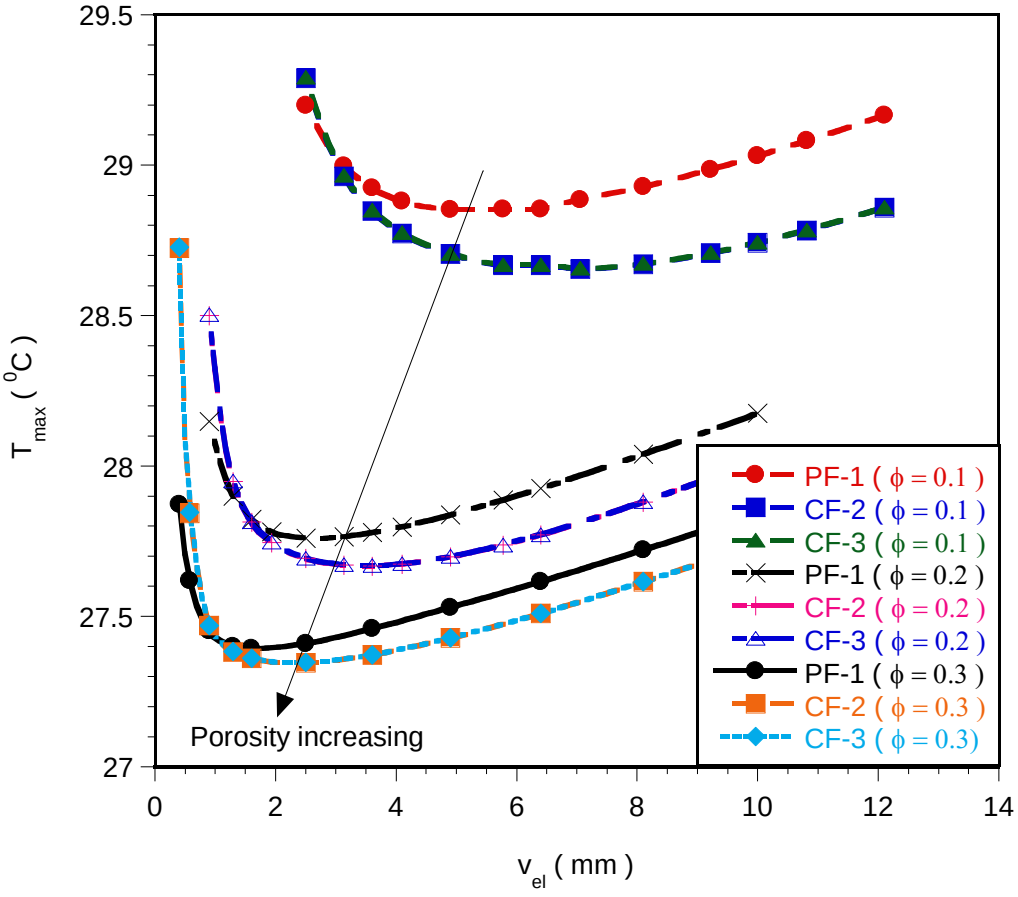

Figure 8. 5 : Effect of the optimised elemental volume on the peak temperature at ΔP = 50 *kPa*

8.6. MATHEMATICAL FORMULATION OF THE OPTIMISATION PROBLEM

In this section, we introduce an optimisation algorithm, Dynamic-Q [208], that will search and identify the design variables at which the system will perform at an optimum.

8.6.1. Optimisation problem and design variable constraints

The optimisation technique described in Chapter 4 was applied to the models described in Section 8.2. The constraint ranges for the optimisation of the three flow orientation configurations are

$$0.125\ \text{mm}^3 \leq v_{el} \leq 20\ \text{mm}^3 \tag{8.8}$$

$$0.1 \leq \phi \leq 0.3 \tag{8.9}$$

$$0 \leq w \leq L \tag{8.10}$$

$$0 \leq d_h \leq w \tag{8.11}$$

$$0 \leq s \leq w \tag{8.12}$$

The optimisation process was repeated for pressure differences across the axial length ranging from 5 *kPa* to 50 *kPa* within the design constraint ranges given in Equations (6.45) to (6.51). This was done in order to search for and identify the channel layout that minimises the peak temperature, $T_{\max}$, such that the minimum thermal resistance between the fixed volume and the cooling fluid is obtained as the desired objectives function.

8.6.2. Mathematical statement of the optimisation problem

The variables chosen for the mathematical statement are

$$x_1 = d_h \tag{8.13}$$

$$x_2 = w \tag{8.14}$$

Substituting Equations (8.13) and (8.14) for Equations (8.8) to (8.12), results in the objective and constraints functions given in Equations (8.15) to (8.17). The inequality functions g_1(x) and g_2(x) are derived from the porosity constraint of Equation (8.6). The mathematical statement of the optimisation problem is then written as

$$f(x) = T_{\max} \tag{8.15}$$

$$g_1(x) = 0.05\pi x_2^{\,2} - x_1^{\,2} \leq 0 \tag{8.16}$$

$$g_2(x) = x_1^{\,2} - 0.3\pi x_2^{\,2} \leq 0 \tag{8.17}$$

8.6.3. Sensitivity analysis of the selection of forward differencing step size

As discussed in Chapter 4. 6, noise exists in any simulation. It is therefore essential to carefully choose a step size Δx to be used in the differencing scheme carefully so that it minimises the noise and gives an accurate representation of the global gradient of the function. A sensitivity analysis was performed by selecting different values of step size for design variables. These values gave a smooth objective function that would later be used as candidate step size. This candidate step size was then verified by running the optimisation program with various starting guesses and checking for any discrepancies in the final solution. Figure 8.6 shows a graph of peak temperature as a function of cooling channel hydraulic diameter with step sizes of 10^{-6} and 10^{-3}. Although, different values of the step size of hydraulic diameter of the cooling

channels as design variable considered are 10^{-6}, 10^{-5}, 10^{-4} and 10^{-3}. A step size of 10^{-3} gave a smooth continuous function of maximum peak temperature and it indeed proved to be an ideal forward-differencing scheme step size for other design variables.

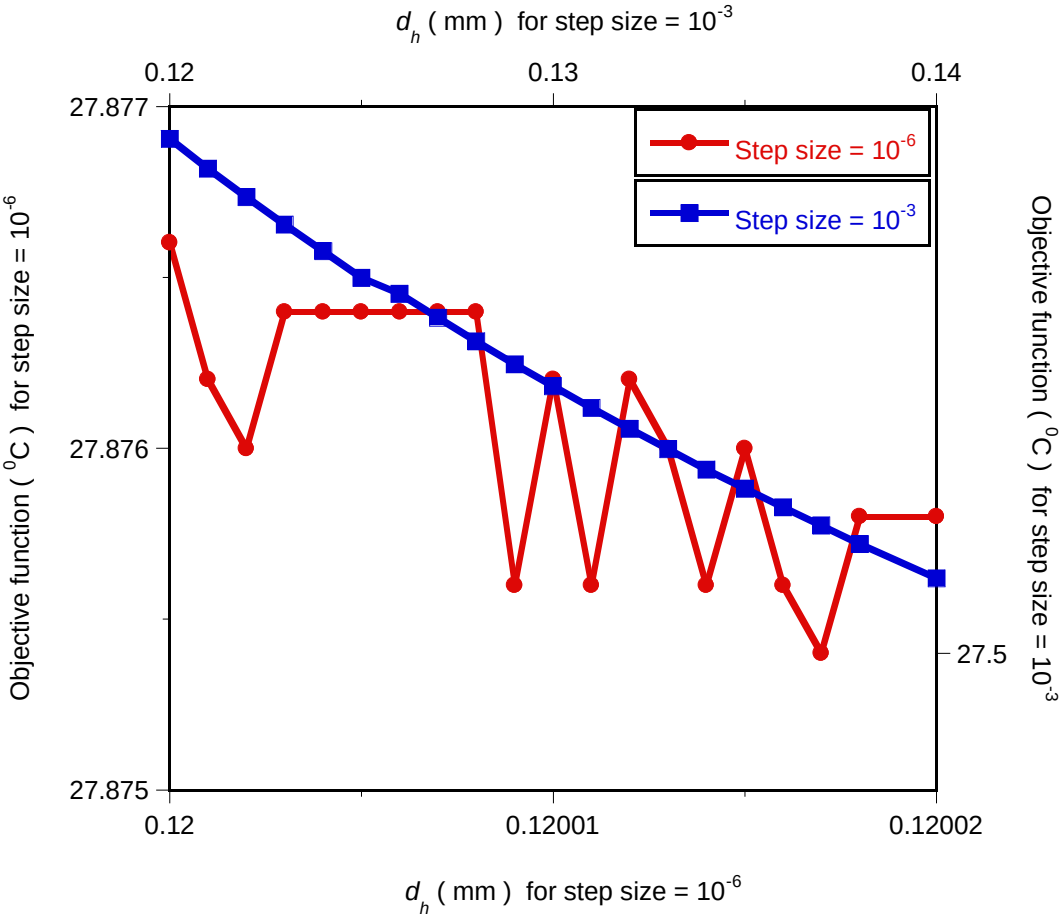

Figure 8. 6 : Plotting peak temperature for different channel width values with step sizes of 10^{-6} and 10^{-3}

Figure 8.7 shows graph of peak temperature as a function of channel-spacing with the chosen candidate step size of 10^{-3}.

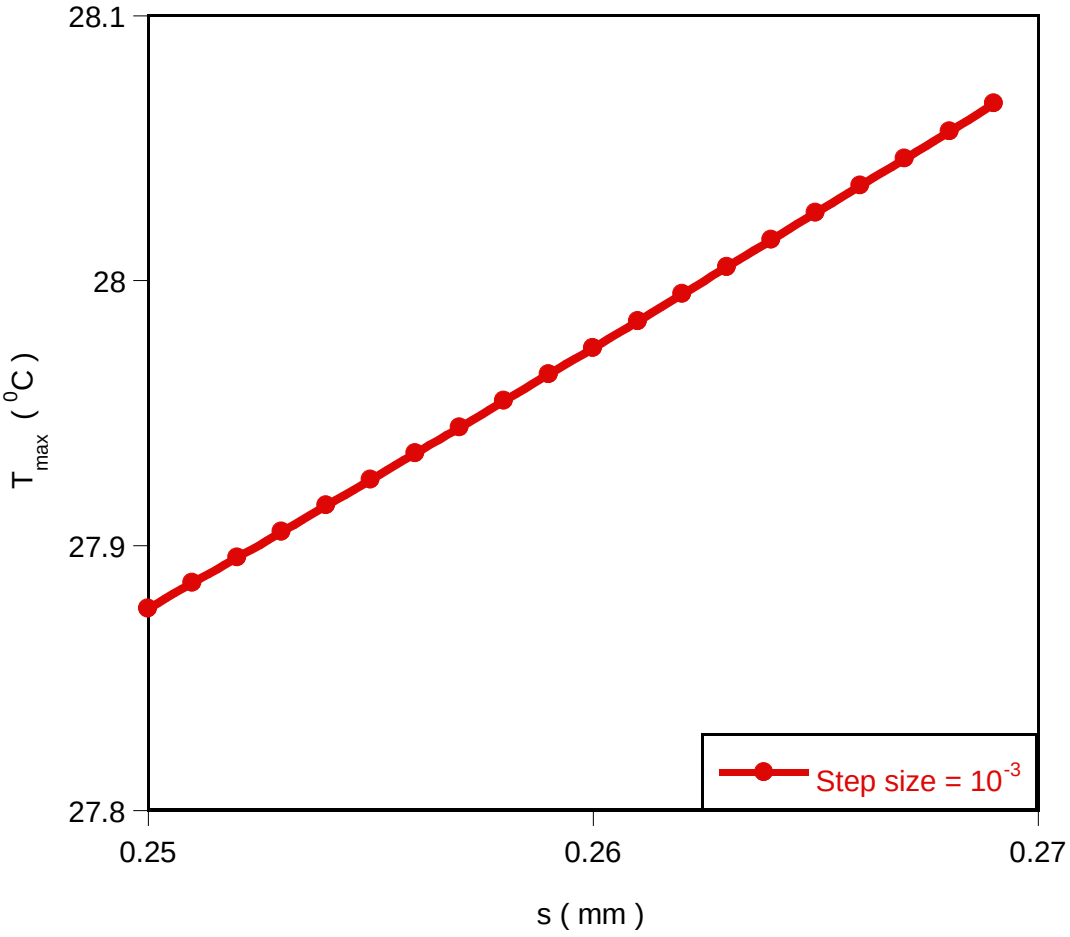

Figure 8. 7: Plotting peak temperature for different channels-spacing values with a step size of 10^{-3}

8.7. OPTIMISATION RESULTS

8.7.1. Effect of the applied pressure difference on optimised geometry and minimised thermal resistance

Figure 8.8 shows the effect of the minimised thermal resistance as a function of applied dimensionless pressure difference for the three flow orientations. The minimised thermal resistance decreases as the applied dimensionless pressure difference and porosity increase. The results also show that the flow orientation has a strong influence on the convective heat transfer. For a specified applied dimensionless pressure difference and porosity, the CF-2 and CF-3 orientations have better performances than the PF1 orientation by 9% for all ranges of porosities and Bejan number used. This is significant enough over a long period of using the CF-2 and CF-3. The CF-2 and CF-3 orientations have almost the same performance. However, the performance of the CF-2 orientation is better than the performance of the CF-3 orientation. Details of the results can be seen in Table 8.4.

Table 8. 4 : Minimised global thermal resistance R_{min} of the three configurations, $R_{\min} \times 10^3$.

	$\phi = 0.1$			$\phi = 0.2$			$\phi = 0.3$		
Be	PF-1	CF-2	CF-3	PF-1	CF-2	CF-3	PF-1	CF-2	CF-3
3.47×10^{9}	0.36	0.33	0.33	0.17	0.15	0.15	0.1	0.092	0.092
6.94×10^{9}	0.26	0.24	0.24	0.12	0.11	0.11	0.071	0.066	0.066
1.39×10^{10}	0.19	0.17	0.17	0.086	0.077	0.077	0.051	0.047	0.047
2.08×10^{10}	0.15	0.14	0.14	0.07	0.063	0.063	0.042	0.038	0.038
2.77×10^{10}	0.13	0.12	0.12	0.061	0.055	0.055	0.036	0.033	0.033
3.47×10^{10}	0.12	0.11	0.11	0.055	0.049	0.049	0.033	0.03	0.03

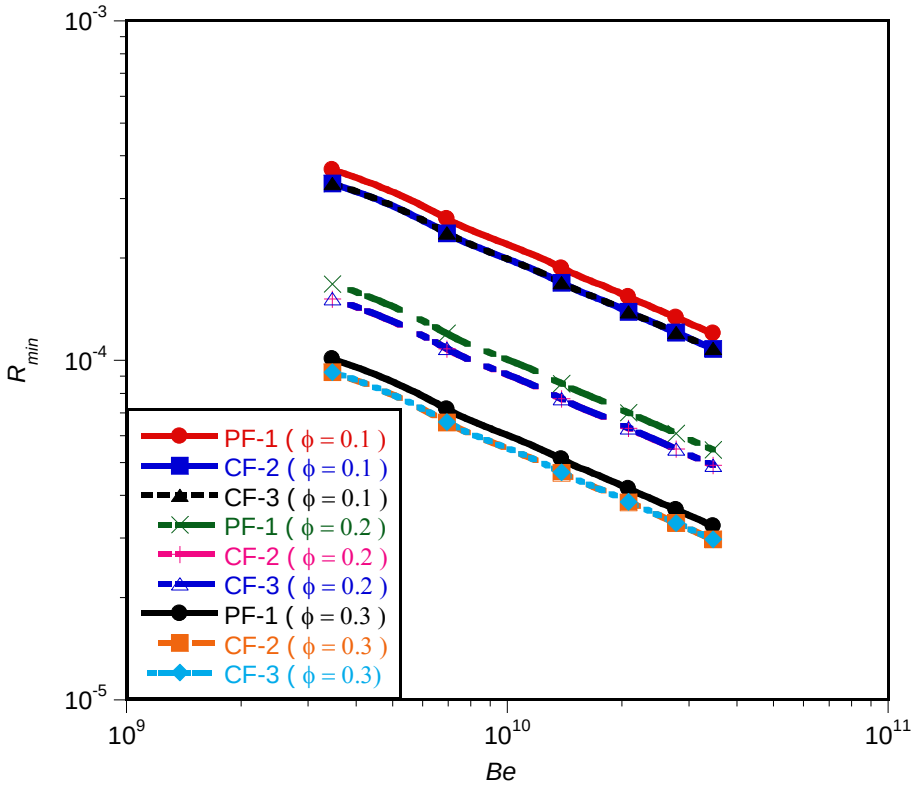

Figure 8. 8 : Effect of dimensionless pressure difference on the minimiseddimensionless global thermal resistance

Figures 8.9 and 8.10 show the behaviour of the geometry with respect to the applied dimensionless pressure difference at different porosities for the three configurations. The optimal hydraulic diameter $d_{h_{opt}}$ decreases as the dimensionless pressure difference increases. There exists an optimal geometry for each of the applied dimensionless pressure differences for the three configurations. According to Figure 8.10, the optimal channel spacing s_{opt} is sensitive to the performance of the system. It

decreases as the dimensionless pressure differences increase and there is a unique optimal spacing for each of the applied dimensionless pressure differences for the configurations. The optimised spacing S_{opt} is directly proportional to the optimised hydraulic diameter $d_{h_{opt}}$. This is also due to the fact that the elemental volume is not fixed, but allowed to morph for a fixed porosity. These results are also in agreement with past research work [94].

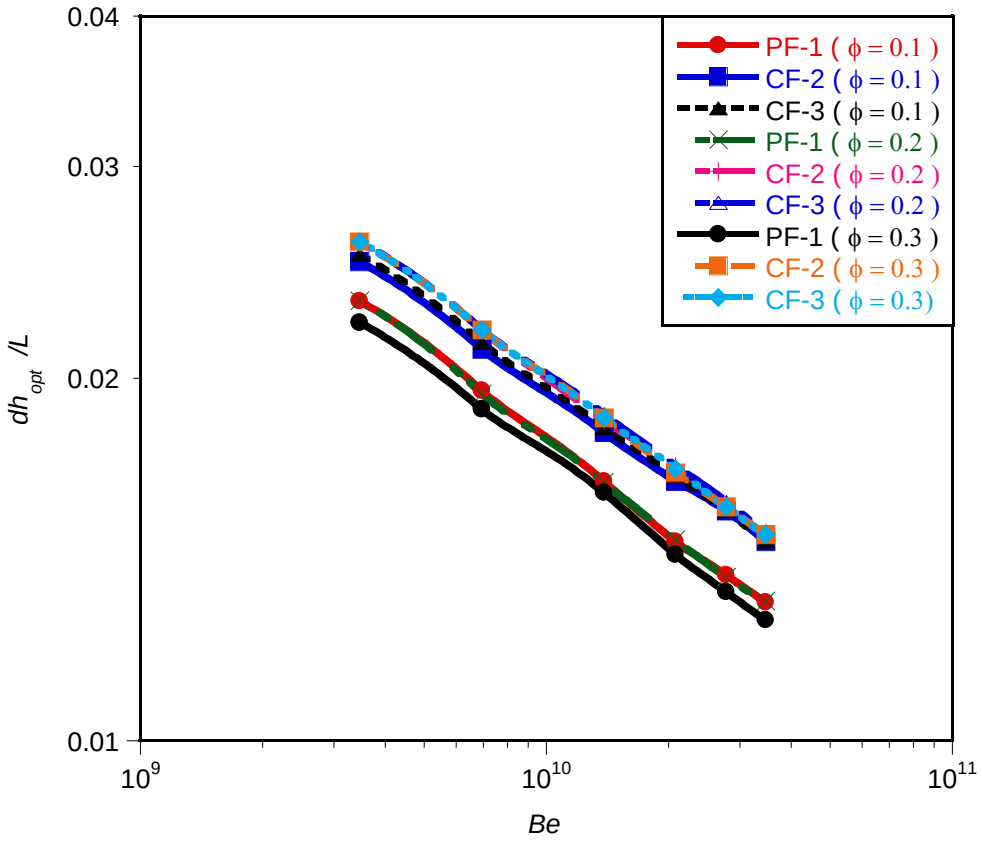

Figure 8. 9 : Effect of dimensionless pressure difference on the optimised hydraulic diameter

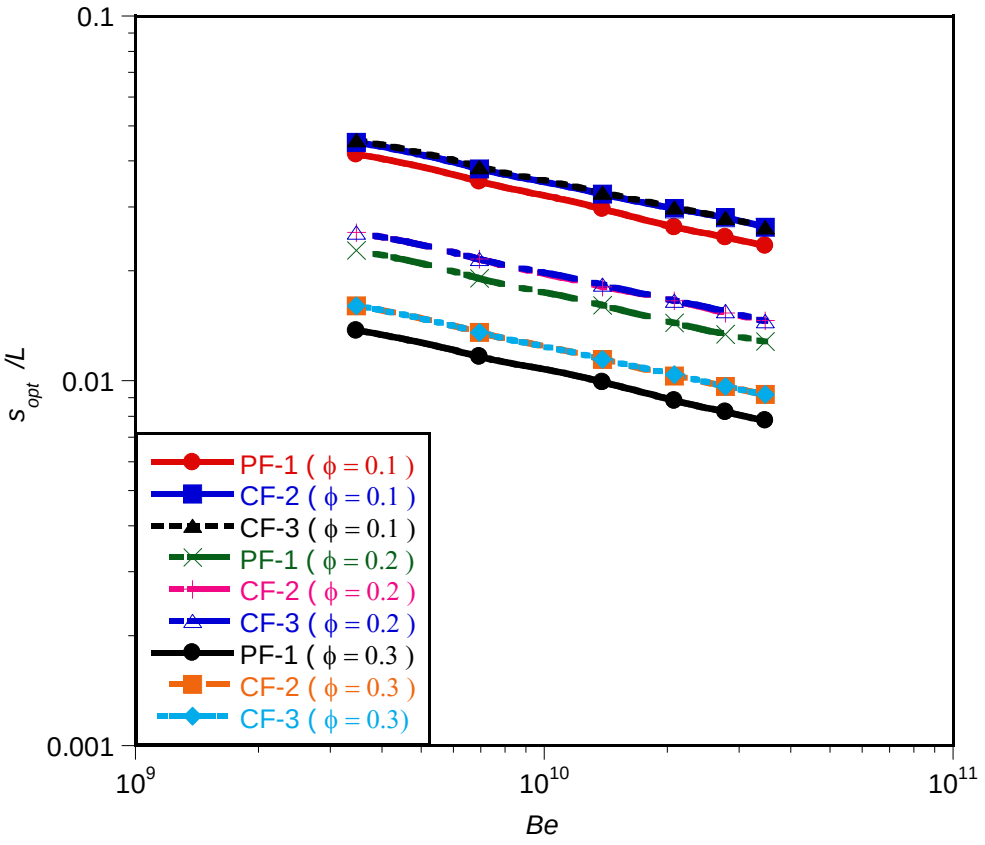

Figure 8. 10 : Effect of dimensionless pressure difference on the optimised channel spacing

8.8. CONCLUSION

This chapter documented the numerical search for geometric structures of conjugate cooling channels in forced convection where internal heat was generated within the solid for an array of parallel cylindrical cooling channels with three flow orientations, PF-1, CF-2 and CF-3.

The configurations were developed in such a way that the peak temperature was minimised subject to the constraint of fixed global volume. The results show that the resulting geometry is a function of the dimensionless pressure difference number. The minimised dimensionless thermal resistance was found to be sensitive to flow orientations. For specified applied dimensionless pressure difference and porosity, the CF-2 and CF-3 orientations perform better than the PF-1 orientation by 9% for all ranges of porosities and Bejan number used. This is significant enough over a long period of using the CF-2 and CF-3. The CF-2 and CF-3 orientations performed almost the same.

The use of the optimisation algorithm coupled with a CFD package made the numerical results robust with respect to the selection of optima geometries, flow orientations of the flow channels and dimensionless pressure difference. Therefore, when designing the cooling structure of heat exchange equipment, the internal and external geometries of the structure, flow orientation and the pump power requirements are very important parameters to be considered in achieving efficient performance.

9

CHAPTER 9: CONCLUSIONS AND RECOMMENDATIONS

9.1. INTRODUCTION

The new trend in modern heat transfer for thermal performance is shape and geometric optimisation. This research was devoted to a study of geometric optimisation of conjugate heat transfer in cooling channels with different cross-sectional shapes, based on constructal theory and design. The objective of the study was to geometrically optimise the cooling structure in such a way that the global thermal resistance or peak temperature between the volume and the cooling fluid would be minimised in heat-generating devices. The configurations of the cooling channels studied were circular, square, isosceles right triangular, equilateral triangular and rectangular.

The research was carried out by performing and developing analytical and numerical analyses of heat transfer for the optimisation of the cooling structure. The analytical solution was based on the asymptotes of intersection method and scale analysis. The numerical simulations, which were guided by the analytical solution, presented a comprehensive explanation of the global thermal behaviour of the problem. To this purpose, computational fluid dynamic software (FLUENT) and mathematical

optimisation algorithms (DYNAMIC – Q) were combined to search for the optimal design variables that would minimise the thermal resistance. The detailed procedures of the theoretical and numerical analyses, as well as the mathematical optimisation algorithms used in this thesis were discussed.

By using the intersection of asymptotes method, the analytical solution provided the existence of an optimal geometry of the external structures and internal architectures of parallel channels of different cross-sectional shapes for cooling volumes that generate heat uniformly. This geometry minimised the global thermal resistance. The numerical modelling section is devoted to a discussion of a set of non-linear partial differential equations governing the transport of mass and heat. The numerical scheme that was implemented in solving the flow and heat transfer was also examined.

The DYNAMIC-Q, which builds on the LFOPC algorithm, presents a multi-dimensional, accurate, reliable and robust penalty method for solving practical constrained engineering design problems and helps to design optimal systems. Numerical noise during simulation and its effect on the gradient-based optimisation algorithms and global performance were also discussed and an efficient way of dealing with the associated problems was suggested.

The analytical and numerical methodology developed in Chapters 3, 4 and 5 were applied to different design cases of cooling channels shapes in heat-generating devices in Chapter 6. The analytical results of Chapter 5 were used to validate the

numerical solutions of Chapter 6. It was found that the numerical and approximate solutions based on scale analysis at optimal geometry dimensions are in good agreement and that the solutions have similar trends. Although the analytical results were lower than the numerical results the theoretical and numerical values agreed within a factor of 1.5 for the worst case. These deviations can be attributed to simplifying assumptions made in the formulation of the theoretical solution.

9.2. CONCLUSIONS

The minimised thermal resistance of all the cooling channels studied is a function of the dimensionless pressure difference number under uniform heat-generation thermal boundary conditions. The minimised thermal resistance decreased monotonically as the applied dimensionless pressure and porosity increased. Also, the optimal geometry is a function of the applied dimensionless pressure number for different configurations. It was shown that a unique optimal geometric configuration exists for a given applied dimensionless pressure difference across a channel which would result in a minimised thermal resistance.

When comparing the shape configurations in Chapter 6, we found that the thermal performance of the circular channel configuration was poorer than any of the other four configurations. An isosceles triangular configuration gave the best thermal performance, followed by the equilateral triangular configuration, the rectangular

shape and square channel. These findings were all in agreement with the analytical solutions provided in Chapter 5.

However, it was clearly observed that cooling was best achieved at a higher aspect ratio of rectangular channels. It was recognised that the optimal design scheme at the higher value of aspect ratio in cross-section for an array of rectangular cooling channels could result in a weaker structure design and increase the difficulty of manufacturing could in fact become impractical due to the channel being too thin.

In Chapter 7, an analytical and numerical CFD package coupled with the optimisation algorithm were used to investigate the geometric optimisation of square cooling channels. These were made of vascularised material with a localised self-cooling property and were subjected to a heat flux on one side in such a way that the peak temperature was minimised at every point in the solid body. The numerical results obtained were in good agreement with the results obtained in the approximate solutions based on a scale analysis at optimal geometry dimensions. The approximate dimensionless global thermal resistance predicted the trend obtained in the numerical results. This showed that there are unique optimal design variables (geometries) for a given applied dimensionless pressure number for fixed porosity.

The material property has a significant influence on the performance of the cooling channel. Therefore, when designing the cooling structure of vascularised material, the internal and external geometries of the structure, material properties and pump power

requirements are very important parameters to be considered in achieving efficient and optimal designs for the best performance.

Chapter 8 documented the numerical search for geometric structures of conjugate cooling channels in forced convection with internal heat generation within the solid for an array of parallel cylindrical cooling channels with three flow orientations, PF-1, CF-2 and CF-3.

The configurations were so developed that the peak temperature was minimised subject to the constraint of fixed global volume. The results show that the resulting geometry is a function of the dimensionless pressure difference number. The minimised dimensionless thermal resistance is sensitive to flow orientations. For specified applied dimensionless pressure difference and porosity, the CF-2 and CF-3 orientations performed better than the PF-1 orientation. The CF-2 and CF-3 orientations performed almost the same.

Therefore, when designing the cooling structure of heat-generating devices or heat exchange equipment, the internal and external geometries of the structure, flow orientation material properties and pump power requirements are very important parameters to be considered in achieving optimal performance.

The use of the optimisation algorithm coupled with the CFD package rendered the numerical results to be more robust with respect to the selection of optima structure

geometries, internal configurations of the flow channels, material properties and pump power requirements.

9.3. RECOMMENDATIONS

The optimisation methodology was applied to the in-line configuration of a cooling channels array. The optimisation can be extended to cooling channels arrays of a staggered configuration. This will enable a comparative study on the minimised thermal resistance analysis and thermal performance capabilities of both configurations. Also, future research may consider the optimisation of additional micro-channels placed in the interstitial regions of an array of cooling channels of different cross-sectional shapes for multi-scale design.

Another interesting extension of this work would be to add one degree of freedom in the system by allowing the tube to have a different diameter while keeping the porosity constant.

Again, future work may investigate the effect of pin fins of any shape transversely arranged along the flow channel of the configurations on the temperature distribution and dimensionless pressure difference characteristics with the global objective of minimising thermal resistance and improving thermal performance.

Furthermore, a study on the effect of temperature-dependent thermo-physical properties of fluid on the minimised thermal resistance is recommended. This is because the thermo-physical properties of some working fluids, such as viscosity, density and thermal conductivity, are sensitive to temperature changes due to relatively large variation of working fluid properties at high heat flux and low Reynolds number (*Re*).

This current research should be extended to the non-Newtonian fluids used in many industries such as the petrochemical, biochemical, pharmaceutical and food industries. This could provide a more comprehensive understanding of the analysis for practical purposes.